A&A 561, A55 (2014)
DOI: 10.1051/0004-6361/201322716

Astronomy & Astrophysics

A Sino-German λ6 cm polarisation survey of the Galactic plane

VIII. Small-diameter sources⋆,⋆⋆,⋆⋆⋆

W. Reich[1], X. H. Sun[1,2,3], P. Reich[1], X. Y. Gao[2], L. Xiao[2], and J. L. Han[2]

[1] Max-Planck-Institut für Radioastronomie, auf dem Hügel 69, 53121 Bonn, Germany
e-mail: wreich@mpifr-bonn.mpg.de
[2] National Astronomical Observatories, CAS, Jia-20 Datun Road, Chaoyang District, 100012 Beijing, PR China
[3] Sydney Institute for Astronomy, School of Physics, The University of Sydney, NSW 2006, Australia

Received 20 September 2013 / Accepted 23 October 2013

ABSTRACT

Aims. Information of small-diameter sources is extracted from the Sino-German λ6 cm polarisation survey of the Galactic plane carried out with the Urumqi 25-m telescope.

Methods. We performed two-dimensional elliptical Gaussian fits to the λ6 cm maps to obtain a list of sources with total-intensity and polarised flux densities.

Results. The source list contains 3832 sources with a fitted diameter smaller than 16′ and a peak flux density exceeding 30 mJy, so about 5× the rms noise, of the total-intensity data. The cumulative source count indicates completeness for flux densities exceeding about 60 mJy. We identify 125 linearly polarised sources at λ6 cm with a peak polarisation flux density greater than 10 mJy, so about 3× the rms noise of the polarised-intensity data.

Conclusions. Despite lacking compact steep spectrum sources, the λ6 cm catalogue lists about 20% more sources than the Effelsberg λ21 cm source catalogue at the same angular resolution and for the same area. Most of the faint λ6 cm sources must have a flat spectrum and are either H II regions or extragalactic. When compared with the Green Bank λ6 cm (GB6) catalogue, we obtain higher flux densities for a number of extended sources with complex structures. Polarised λ6 cm sources density are uniformly distributed in Galactic latitude. Their number density decreases towards the inner Galaxy. More than 80% of the polarised sources are most likely extragalactic. With a few exceptions, the sources have a higher percentage polarisation at λ6 cm than at λ21 cm. Depolarisation seems to occur mostly within the sources with a minor contribution from the Galactic foreground emission.

Key words. radio continuum: general – polarization – catalogs

1. Introduction

Diffuse continuum emission is highly concentrated in a narrow band along the Galactic plane, where the number density of discrete Galactic sources, such as supernova remnants (SNRs) and H II regions, is the highest. Recently, the maps from the Sino-German λ6 cm polarisation survey of the Galactic plane have been published in a series of papers (Sun et al. 2007, 2011a; Gao et al. 2010; Xiao et al. 2011). The survey also served as one basis for a systematic study of known SNRs (Sun et al. 2011b; Gao et al. 2011b) and for a search for new ones (Gao et al. 2011a). Han et al. (2013) summarise the λ6 cm survey project and the results obtained so far. This paper adds a catalogue of discrete small-diameter sources in the surveyed area, including polarised sources.

At λ6 cm, optically thin diffuse thermal emission dominates in the Galactic plane, while diffuse steep-spectrum synchrotron emission dominates at longer wavelengths. Thus, faint H II regions are expected to be better separable and therefore identified from the diffuse emission at λ6 cm than in the single-dish surveys carried out with the Effelsberg 100-m telescope at λ21 cm (Reich et al. 1990b, 1997) and λ11 cm (Reich et al. 1984, 1990a; Fürst et al. 1990a). On the other hand, the extraction of faint steep-spectrum extragalactic sources from the diffuse Galactic emission becomes more difficult at λ6 cm. In any case, λ6 cm flux densities are a valuable addition to existing longer wavelength data, and a more precise spectral index determination is provided when the wavelength difference increases.

Synthesis telescope source surveys, such as the most sensitive NRAO VLA Sky Survey (NVSS; Condon et al. 1998) at λ21 cm, list many more compact sources along the Galactic plane compared to published single-dish surveys. These observations have much higher angular resolution and sensitivity. They filter out extended Galactic emission and also may underestimate the integrated flux density of extended sources.

Previously, an important λ6 cm source survey of the northern sky, the GB6, had been carried out with the former Green Bank 300-ft telescope with an angular resolution of 3.′6 × 3.′4 by Condon et al. (1994). The corresponding source catalogue (Gregory et al. 1996) includes compact sources up to 10.′5. The peak flux density increases with declination with a lower limit of 18 mJy (Gregory et al. 1996). In the reduction process of the GB6 survey, spline functions were used to subtract all kind of extended emission from the raw data, which includes Galactic emission. Therefore the maps in the Galactic plane can not be compared with those from the present λ6 cm survey. The GB6 survey processing should not affect the flux

⋆ Table 2 is available in electronic form at http://www.aanda.org
⋆⋆ Table 2 is also available at the CDS via anonymous ftp to cdsarc.u-strasbg.fr (130.79.128.5) or via http://cdsarc.u-strasbg.fr/viz-bin/qcat?J/A+A/561/A55
⋆⋆⋆ Full Table 1 is only available at the CDS via anonymous ftp to cdsarc.u-strasbg.fr (130.79.128.5) or via http://cdsarc.u-strasbg.fr/viz-bin/qcat?J/A+A/561/A55

density determination of compact sources, what can be proved by comparison with the present catalogue.

Lists of polarised sources in the Galactic plane are rare and do not exist at all at λ6 cm. For λ21 cm, however, several data sets exist: The NVSS (Condon et al. 1998) includes polarisation information. Brown et al. (2003) provides polarisation data from the Canadian Galactic Plane Survey (CGPS) and Van Eck et al. (2011) presents a list of polarised sources along the Galactic plane measured with the VLA, which could be compared with the λ6 cm polarisation data. The Effelsberg λ21 cm and λ11 cm survey source lists (available from the CDS/Strasbourg[1]) have guided us in the layout of the λ6 cm source list, where all relevant parameters of individual sources are provided. In Sect. 2, we summarise the λ6 cm survey project and describe the source fitting procedure in Sect. 3. In Sect. 4, we present the list of sources and describe their individual parameters. In Sect. 5, we briefly discuss the λ6 cm source catalogue with respect to source statistics and other available catalogues and make concluding remarks in Sect. 6.

2. The λ6 cm survey

The Sino-German λ6 cm polarisation survey of the Galactic plane was conducted with the Urumqi 25-m telescope of Xinjiang (formerly Urumqi) Astronomical Observatory, Chinese Academy of Sciences, between 2004 and 2009. The surveyed area covers $10° \leq l \leq 230°$ and $-5° \leq b \leq +5°$. The survey has an angular resolution of $9\rlap{.}'5$. The system temperature towards the zenith was about 22 K. The central frequency was set to either 4.8 GHz or 4.963 GHz with corresponding bandwidths of 600 MHz and 295 MHz. The system gain is $T_{\rm B}$[K]/S[Jy] = 0.164. Detailed information about the receiving system, the survey set-up, and its reduction scheme has already been presented by Sun et al. (2007). The survey maps were published in three sections by Gao et al. (2010); Sun et al. (2011a); Xiao et al. (2011) and are also available on the web[2].

The Galactic plane was fully sampled at $3'$ and mapped by raster scans in the longitude and latitude directions. The primary calibrator was 3C 286 with an assumed flux density of 7.5 Jy and a polarisation percentage of 11.3%. The polarisation angles measured for 3C 286 were found as $32° \pm 1°$ and were not corrected to the nominal value of 33°. Then 3C 48 and 3C 138 were used as secondary calibrators, and 3C 295 and 3C 147 as unpolarised calibrators. Sun et al. (2007) found a scaling accuracy of better than 4% for total intensities and 5% for polarised intensities.

The raw data from the receiving system contain maps of I, U, and Q stored in NOD2-format (Haslam 1974). Data processing follows the standard procedures developed for continuum observations with the Effelsberg 100-m telescope as detailed by Sun et al. (2007) and Gao et al. (2010). The positional accuracy of compact sources in the survey maps was found to be in general better than $1'$ when compared with the high-resolution interferometric NVSS survey (Condon et al. 1998). Maps with larger position offsets were corrected with respect to the NVSS source positions. The final survey maps have a typical measured rms noise including confusion of about 1 mK $T_{\rm B}$ or 6.1 mJy/beam area for total intensity I, 0.5 mK $T_{\rm B}$ or 3.05 mJy/beam for Stokes U and Q, and polarised intensity PI.

[1] http://vizier.u-strasbg.fr

[2] http://zmtt.bao.ac.cn/6cm/

3. Source fitting procedure

3.1. Total intensity fit

We used the same Gaussian fitting routine applied to extract compact sources from the Effelsberg λ21 cm (Reich et al. 1990b, 1997) and λ11 cm survey maps (Reich et al. 1984; Fürst et al. 1990b) to produce a list of compact sources from the λ6 cm survey maps. This is the standard NOD2-based fitting routine for continuum and polarisation observations with the Effelsberg 100-m telescope, which has a Gaussian beam shape up to mm-wavelengths.

The fitting routine can be steered in various ways. The standard procedure is to run an automatic fit on a map, where a small area around each source is extracted and corrected for baseline gradients before a fit is applied, which is either a circular or an elliptical Gaussian. The highest peaks in a map are fitted in a first run, and subsequently the peak amplitude limit is decreased. It turns out, that for most λ6 cm sources, the automatic procedure does not give the best result as seen by the residual emission after source subtraction, so that most sources were fitted individually from the maps by defining the area for the fit where confusing surrounding emission is excluded as well as possible.

The inner Galactic plane has steep intensity gradients in Galactic latitude, which makes it difficult to extract faint sources. In analogy to the treatment of the Effelsberg survey maps, we applied the "unsharp-masking" filtering method by Sofue & Reich (1979) by using a 1° wide filtering beam to remove most of the diffuse emission before applying the source fitting routine, which improves the number of separable sources from unrelated emission and also improves the fit result. The peak flux amplitude limit was taken as 5× the rms noise, e.g. 5 mK $T_{\rm B}$ or 30 mJy/beam area. In addition we rejected all source fits with the minor axis below $6'$, which indicates either an RFI-spike, another small-scale distortion, or surroundings that are too complex. Also, fit results of the major axis exceeding $16'$ were rejected, which is the same limit as used earlier for the Effelsberg λ21 cm source list with about the same beam size. For sources that are significantly larger than the angular resolution, the application of a single Gaussian fit becomes questionable, because source shapes are complex in general. This is visible by residual emission structures after source subtraction.

We checked the reliability of the listed sources by comparing with the corresponding Effelsberg λ21 cm (Reich et al. 1990b, 1997) and λ11 cm source lists (Fürst et al. 1990b). We also compared $1° \times 1°$ λ6 cm maps centred on each source with the corresponding Effelsberg maps at λ21 cm and λ11 cm to check their reliability further and to identify misidentifications by low-level distortions. A number of sources with poor fits shown by large formal errors could be identified as artificial. There are well-fitted λ6 cm sources, which are barely or not at all visible in the longer wavelengths surveys.

3.2. Fit of linearly polarised sources

Separating the small-scale emission of polarised sources is not trivial in the presence of significant extended polarised emission. We started from the observed Urumqi λ6 cm Stokes U and Q maps, which included extended polarised emission structures of up to a few degrees in size. We removed the large-scale components by applying the filtering method by Kothes & Kerton (2002), which is a modification of the Sofue & Reich (1979) filter and separates positive *and* negative small-scale structures from large-scale emission. The Sofue & Reich (1979) filter only

Table 1. Flux densities of 3832 compact sources at λ6 cm.

No.	L (D)	B (D)	RA (2000) (H M S)	Dec (2000) (D ′ ″)	Flux (mJy)	Peak flux (mJy)	Size and p.-angle	Error class
1	10.085	0.742	18 5 10.7	−19 51 13	573	514	SE	222
2	10.161	−0.347	18 9 23.2	−20 19 3	63 835	43 890	12.7/10.3/28	2121
3	10.268	3.344	17 55 59.5	−18 24 22	64	54	SE	224
4	10.311	−0.117	18 8 50.4	−20 4 29	15 923	13 252	SE	323
5	10.324	0.897	18 5 6.1	−19 34 10	124	124	PL	234
6	10.632	−0.390	18 10 31.0	−19 55 33	10 250	7654	SE	112
7	10.698	−3.168	18 21 5.5	−21 11 20	235	173	12.2/10.0/99	2121
8	10.793	−0.875	18 12 39.4	−20 1 5	791	530	12.2/11.0/39	2241
9	10.819	3.481	17 56 39.0	−17 51 41	99	80	SE	246
10	10.931	−3.880	18 24 15.6	−21 18 54	85	71	SE	223
11	10.971	3.004	17 58 42.4	−17 58 3	404	404	PL	222
12	11.063	−2.597	18 19 39.9	−20 35 56	234	165	12.7/10.1/72	2231
13	11.167	−0.356	18 11 29.2	−19 26 27	9423	8036	SE	111
14	11.196	0.118	18 9 47.1	−19 11 12	2168	1635	SE	234
15	11.200	−1.087	18 14 16.6	−19 45 44	4234	2107	14.5/12.5/59	2121
16	11.235	3.512	17 57 24.4	−17 29 10	150	112	11.8/10.3/94	1121
17	11.303	−4.756	18 28 20.0	−21 23 25	360	322	SE	212
18	11.360	4.330	17 54 42.0	−16 58 9	156	134	SE	222
19	11.423	−0.063	18 10 55.2	−19 4 31	3586	2229	13.7/10.6/116	1121
20	11.509	3.182	17 59 10.6	−17 24 46	186	138	11.1/10.9/144	2121
21	11.555	0.363	18 9 36.8	−18 45 14	605	540	SE	222

Notes. The full table is available in electronic form at the CDS.

separates positive small-scale and large-scale emission and is only applicable to total intensity or polarised intensity maps. We filtered the Stokes U and Q survey maps with a filtering beam of 30′ and calculated PI-maps via $PI = (U^2 + Q^2)^{0.5}$. For all sources identified in total intensity, we extracted 1° × 1° large fields centred on the source position in PI and applied a Gaussian fit, which takes the positive PI noise bias into account. Polarised peak flux densities of 10 mJy or higher were accepted. This limit is slightly above 3× the rms-noise of polarised emission. The lowest percentage polarisation in our list is 1.8%. We did not include sources close to the level of instrumental polarisation of the Urumqi telescope, which was found to be of about 1% after cleaning, as discussed by Sun et al. (2011a). For polarised sources, we also fitted the U and Q maps to calculate the Galactic polarisation angle PA by $PA = 0.5$ atan (U/Q). When either the U or Q value could not be fitted by a Gaussian, we estimated its amplitude from a scan across the peak of the source.

4. The source list

4.1. Total-intensity data

We list the parameters of the 3832 catalogued sources in Table 1, which is accessible from the CDS in Strasbourg.

From the Gaussian fit of each source, we calculated its integrated flux density $S_{\rm i}$ assuming a Gaussian shape using the fitted peak flux density $S_{\rm p}$ and the major $\theta_{\rm max}$ and the minor $\theta_{\rm min}$ axis of the ellipsoid by $S_{\rm i} = S_{\rm p} \times (\theta_{\rm max} \times \theta_{\rm min} \times HPBW^{-2})$, with $HPBW = 9\rlap{.}'5$. We quote the fitted sizes in Table 1. For Gaussian-shaped sources, the intrinsic size calculates as source-size = (fitted size^2 − $HPBW^2)^{0.5}$. The positional accuracy of the λ6 cm survey was checked using the positions of NVSS sources as reference for each survey map (Sun et al. 2007). If necessary, they were corrected for a position accuracy of better than 1′. This error is not included in the positional uncertainty from the Gaussian fit listed in Col. 9 of the source table. The integrated flux density error does not include the survey scaling error of less than 4%. As for the Effelsberg λ21 cm and λ11 cm source lists, we use error classes to quantify the errors from the Gaussian fit.

The source table includes the following data:

- Col. 1: sequential number;
- Cols. 2 and 3: Galactic longitude and latitude;
- Cols. 4 and 5: right ascension and declination (J2000);
- Col. 6: integrated flux density in mJy;
- Col. 7: peak flux density in mJy;
- Col. 8: PL – point-like source: fitted size smaller than 10′ × 10′;
  SE – slightly extended source: fitted size smaller than 11′ × 11′;
  for extended sources:
  1. number: fitted FWHM along the major axis in arcmin;
  2. number: fitted FWHM along the minor axis in arcmin;
  3. number: Galactic position angle of the source ellipsoid;
- Col. 9: error class of the fitting procedure:
  1. digit: positional error in units of 5″;
  2. digit: integrated flux density error in units of 5%;
  3. digit: size error in units of 10″;
  4. digit: error of the Galactic position angle in units of 1°.

From the small-diameter SNRs in the λ6 cm survey, which were discussed by Sun et al. (2011b), a number of sources have apparent sizes below the limit of 16′ and were thus included in Table 1. The integrated flux densities from Gaussian fitting and the ring integrations performed by Sun et al. (2011b) in general agree within the quoted errors. For a few cases, the different methods lead to flux density differences, which slightly exceed the quoted errors. The complex surrounding of G11.1−1.0 (source 15), for example, leads to a lower integrated flux density by ring integration (3.40 ± 0.25 Jy) than by the Gaussian fit (4.234 ± 0.212 Jy). The same is found for G74.9+1.2 (source 1085), where ring integration gives 6.35 ± 0.35 Jy and the Gaussian fit 7.217 ± 0.361 Jy. SNR G59.8+1.2 (source 819) has a slightly lower Gaussian flux density (1.17 ± 0.06 Jy) than obtained by ring integration (1.43 ± 0.08 Jy), which, however, includes its tail. Some listed sources within the area of SNRs are either compact substructures or unrelated background sources. Their flux densities are therefore always below that of the SNR. An example for a Gaussian fit of a substructure is G16.8−1.1 with 3.91 Jy (source 87) versus 7.39 Jy for the entire object (Sun et al. 2011b). Table 1 also contains a few sources in the area of large-diameter SNRs studied by Gao et al. (2011b), where it is not always clear whether they are unrelated background sources or compact substructures of the SNRs.

4.2. Polarised sources

We list 125 polarised λ6 cm sources in Table 2, which is also available at the CDS in Strasbourg. Table 2 includes some total-intensity information from Table 1 and the following data:

- Col. 1: sequential number from Table 1;
- Cols. 2 and 3: Galactic longitude and latitude (L, B) in degrees from Table 1;
- Cols. 4 and 5: integrated ($S_{\rm i}$) and peak flux density ($S_{\rm p}$) in mJy from Table 1;
- Col. 6: polarised peak flux density ($\mathrm{PI_p}$) in mJy/beam;
- Col. 7: Galactic polarisation angle ($\mathrm{PA_{gal}}$) in degrees;
- Col. 8: equatorial polarisation angle for epoch 2000 ($\mathrm{PA_{J2000}}$) in degrees;
- Col. 9: peak percentage polarisation ($\mathrm{PC_p}$);
- Col. 10: remarks: identifications (see text), PC21 (percentage polarisation at λ21 cm available).

We list polarised peak flux density ($\mathrm{PI_p}$), the Galactic and equatorial polarisation angles ($\mathrm{PA_{gal}}$, $\mathrm{PA_{J2000}}$), and the peak percentage polarisation ($\mathrm{PC_p}$). The polarised flux densities were obtained from the PI maps with the same Gaussian fitting software as used for the total-intensity fits. The quoted extent from the Gaussian fit of the total-intensity and the much fainter polarised emission often differ, so that we quote peak flux densities rather than integrated flux density values. To obtain integrated polarised intensity values for extended objects, the public survey maps should be used and intensity integrations performed. We have excluded the extended sources 84 (l, b = 16.518, −3.226), 401 (l, b = 36.686, 1.831), and 415 (l, b = 37.429, −2.430) from Table 2, for which we obtained formal percentage polarisations exceeding 35%. These sources are all located towards the inner Galaxy, where polarised emission is rather patchy, so that chance coincidences of an unrelated polarised patch with a weak source may happen. These three sources are all visible in the Effelsberg surveys, but are faint and not listed as discrete sources. No further spectral or other information is available for these sources from VizieR at the CDS in Strasbourg.

In Col. 9, we have added identifications taken from the CDS, where SNR stands for supernova remnant, HII for H II region, PN for planetary nebula, RadGal for radio galaxies, QSO for quasars, and AGN for active galactic nuclei, where "AGN?" indicates candidate objects. The well-studied 3C sources were also included. For most sources, λ21 cm percentage polarisation is available, which we have marked as PC21 in Table 2. Most of these data come from the NVSS (Condon et al. 1998), a few from the CGPS (Brown et al. 2003) and from the VLA (Van Eck et al. 2011). Polarisation data from Broten et al. (1988) and Tabara & Inoue (1980) were also used.

A few polarised sources listed in Table 2 refer to known SNRs, SNR substructures, or sources in their area. The polarised λ6 cm emission from SNRs in the surveyed region has already been studied by Sun et al. (2011b) and by Gao et al. (2011b). The polarised emission from G76.9+1.0 could not be determined by ring integration (Sun et al. 2011b), where a Gaussian fit (source 1120) reveals a PC of 4.0%. For 3C 58 (source 2052), the Gaussian fit gives 4.7% instead of 6% by ring integration. For the SNRs G39.2−0.3 (source 439) and G74.9+1.2 (source 1085), the percentage polarisations obtained from both methods agree. Sources 2942 (l, b = 179.473, 2.624) and 2976 (l, b = 181.440, −2.125) are located along the shells of G179.6+2.0 (Gao et al. 2011b) and SNR S147 (Xiao et al. 2008), respectively. The sources 3185 (l, b = 192.352, 0.372) and 3223 (l, b = 194.527, 2.685) are located in the direction of the "Origem Loop", which has recently been shown by Gao & Han (2013) to consist of a polarised arc in the north, most likely a part of an SNR, and H II regions in the south. The extended source 3185 is located near a bright H II region with detected infrared emission, but not identified so far. Source 3223 has a steep spectrum and is most likely extragalactic.

The sources 3C 154 (source 3070, l, b = 185.592, 4.002), 3C 410 (source 1004, l, b = 69.209, −3.763), and also source 3208 (l, b = 193.652, 4.395) were observed with the Effelsberg 100-m telescope at λ6 cm (Reich et al. 2000), including polarisation to study the radio properties of ROSAT X-ray sources. They measured 4% for 3C 154 versus 4.3% (source 3070) in Table 2. For 3C 410 Reich et al. (2000) quote 3% in agreement with 3.3% (source 1004). For source 3208, a steep-spectrum AGN, Reich et al. (2000) measured 9% at λ6 cm versus 5% in the present list. The equatorial polarisation angles of the three sources listed in Table 2 agree within 4° with those measured by Reich et al. (2000).

5. Discussion

The aim of this paper is to present the λ6 cm source catalogue in total and polarised intensity. The following brief discussion demonstrates the impact of the new catalogue in view of existing data sets. Using catalogues at various frequencies from different telescopes with large differences in angular resolution to calculate source properties, such as their spectra, may be a difficult exercise in practice. Vollmer et al. (2010) present SPECFIND V2.0 (accessible via the CDS/Strasbourg), which is a systematic approach to deriving about 65×10^3 spectra of radio sources. They show examples for the general large scatter in published flux densities, but also discuss methods for deriving reliable spectra.

5.1. Total-intensity data

5.1.1. Source statistics

The distribution of λ6 cm sources as a function of Galactic latitude and absolute latitude is shown in Fig. 1. For Galactic longitudes less than 100°, a concentration of extended sources within 1° latitude is visible, which is similar to the Effelsberg λ11 cm extended source distribution (see Fürst et al. 1990b, Fig. 4), which is slightly wider in latitude. This is a clear indication that extended sources are mostly of Galactic origin. The "PL" and "SE" source distribution is almost latitude independent, indicating that most of these sources are extragalactic. For longitudes above 100°, the distribution shows no clear latitude dependence for all source classes, again this agrees with the distribution of λ11 cm sources (see Fürst et al. 1990b, Fig. 5). We conclude that sources classified as "extended", e.g. with fitted sizes above 11′ are mostly Galactic. Their density is highest

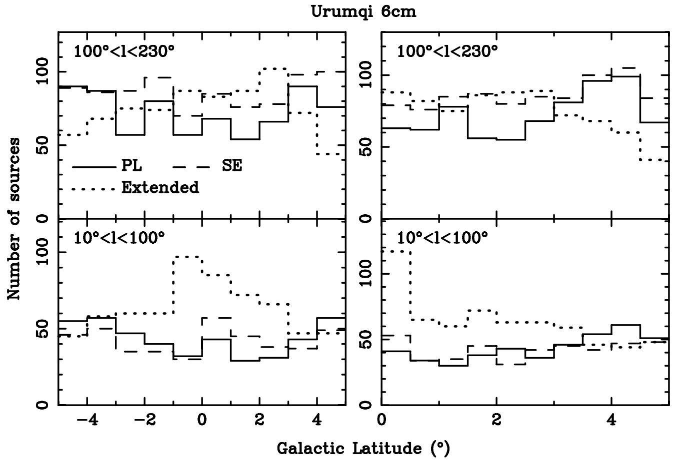

Fig. 1. Latitude (*left*) and absolute latitude distribution (*right*) for the three source classes, "PL", "SE", and "Extended", shown for the inner and outer Galaxy.

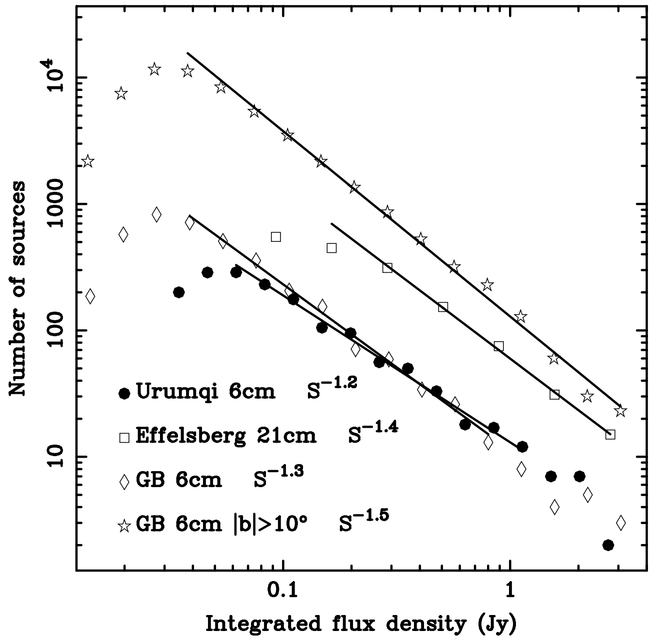

Fig. 2. Cumulative source counts in the anti-centre for "PL" and "SE" sources from the indicated catalogues. We also show the GB6 compact source count outside of the Galactic plane.

within absolute latitudes of 1° towards the inner Galaxy, where the diffuse Galactic emission also peaks.

Fürst et al. (1990b) presented cumulative source counts at λ11 cm for longitudes from 100° to 240° by counting "PL" and "SE" sources, where the majority are extragalactic. The slope of the source count distribution was fitted by $S^{-1.4}$, which is close to $S^{-1.5}$ as expected for an isotropic source distribution. The same is found for the Effelsberg λ21 cm "PL" and "SE" sources for the area from 100° to 230° as shown in Fig. 2. The source counts for the Urumqi "PL" and "SE" sources and the GB6 compact λ6 cm sources, excluding border sources (B flag), extended (E flag) and weak sources with large zero-level (W flag), and also sources near a strong source (C flag) (Gregory et al. 1996), are included in Fig. 2. They show a slightly flatter slope, possibly indicating an increase in the fraction of Galactic sources at shorter wavelengths or selection effects by confusion. The high-latitude compact GB6 source count for latitudes over 10° is fitted by $S^{-1.5}$ (Fig. 2). The Galactic plane source numbers drop below the fit for flux densities lower than about 40 mJy for GB6 and 60 mJy for Urumqi λ6 cm sources. Below these flux density levels, the catalogues become incomplete.

5.1.2. Comparison with the Effelsberg λ21 cm source list

The angular resolution of the Sino-German λ6 cm polarisation survey of 9.′5 matches that of the λ21 cm survey of 9.′4 carried out with the Effelsberg 100-m telescope (Reich et al. 1990b, 1997). The source lists from both surveys are limited to source sizes of 16′.

The minimum peak flux density limit of the λ21 cm source list for the anti-centre area for longitudes over 95.°5 (Reich et al. 1997) was 79 mJy, while it was 98 mJy for longitudes below 95.°5 (Reich et al. 1990b). For a λ21 cm peak flux density limit of 98 (79) mJy, non-thermal sources with spectral indices larger than $\alpha = -1.0$ (-0.8) ($S \sim \nu^{\alpha}$) should be detected and included in the λ6 cm source list. Fainter sources or sources with a steeper spectrum will be missed. The spectral index distribution for Westerbork Northern Sky Survey (WENSS; Rengelink et al. 1997) sources at 327 MHz and NVSS sources at 1.4 GHz derived from about 186 000 sources by Zhang et al. (2003) shows that about 40% of compact sources have spectra steeper than $\alpha = -1.0$. Thus, a significant fraction of compact λ21 cm sources will be missed at λ6 cm. On the other hand, flat-spectrum sources with a λ6 cm peak flux density below 90 (70) mJy will be missed at λ21 cm. Some extended sources might be missed, when they slightly exceed the size limit in one catalogue, but were just below in the other.

In the latitude limits of ±4° of the Effelsberg λ21 cm inner Galactic plane survey and longitudes between 10° and 95.°5, we find 1127 sources at λ6 cm, while the λ21 cm source list has 827 entries. Among them 673 sources are listed in both catalogues. In the anti-centre area, for longitudes higher than 95.°5, we find 1950 sources at λ6 cm compared to 1643 sources at λ21 cm, where 1414 λ6 cm sources have a counterpart in the λ21 cm catalogue.

All together, the λ6 cm source list contains about 20% more sources than the λ21 cm source list. From the mentioned selection effects, we conclude that most of the faint λ6 cm sources must be flat-spectrum synchrotron sources or optically thin thermal sources. This is a significant fraction of sources in the Galactic plane at λ6 cm.

The λ21 cm and λ6 cm surveys have about the same angular resolution, which allows us to calculate spectral indices with peak flux densities rather than integrated flux densities, where differences in the fitted sizes at the two wavelengths decrease the accuracy. We show the result for sources listed in both catalogues in Fig. 3. The two lines indicate spectral indices of $\alpha = -0.80$ and $\alpha = -0.07$, which were derived from a double Gaussian fit. Some clustering of sources along these lines is seen. Extragalactic sources have a median spectral index of $\alpha \approx -0.9$ (Zhang et al. 2003). Figure 3 shows that most of the strong sources have a flat spectrum with $\alpha \approx -0.1$.

5.1.3. Comparison with the GB6 source list

The λ6 cm multi-beam source survey carried out with the former 300-ft Green Bank Telescope (Condon et al. 1994) has an angular resolution of 3.′6×3.′4. We compared the GB6 integrated flux densities from the catalogue compiled by Gregory et al. (1996) with the present source list. The Gregory et al. (1996)

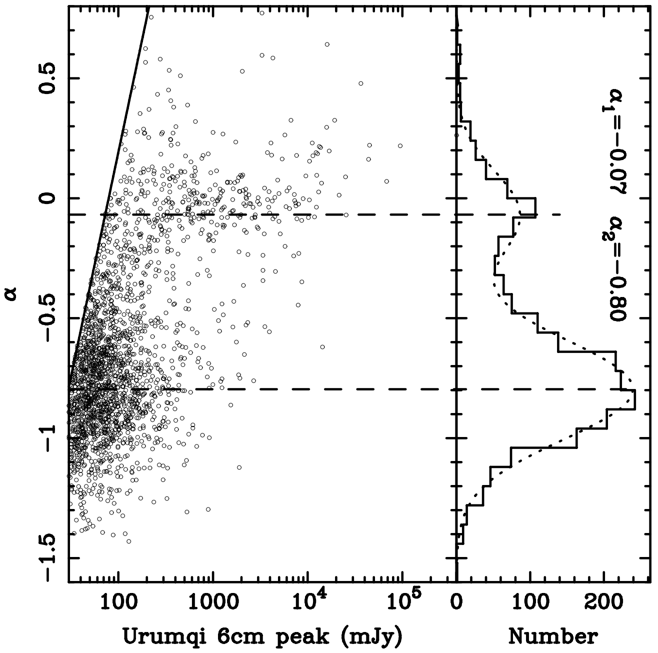

Fig. 3. Spectral indices calculated from Effelsberg λ21 cm and Urumqi λ6 cm peak flux densities. The solid line in the *left panel* indicates the spectral indices derived from the λ6 cm peak flux densities and the peak flux density limit of 79 mJy at λ21 cm. The two dashed lines show the peak locations from double Gaussian fitting in dotted lines in the *right panel*.

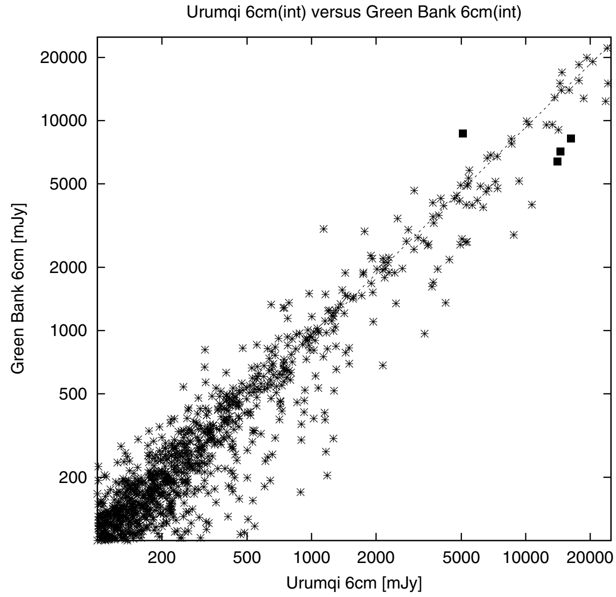

Fig. 4. Comparison of integrated flux densities from the present λ6 cm catalogue with those from the GB6 source list. Four sources with large flux differences are marked by squares and were discussed in the text.

catalogue includes sources up to 10′.5 in size. The present λ6 cm source list includes sources with sizes up to 13′. We took into account that for a small number of objects the GB6 catalogue lists two sources because of its higher angular resolution. Their flux densities were added for the comparison. In cases where the two GB6 sources have a positional difference of a few arcminutes, the Gaussian fit of a single extended source has a large error and the residuals are large. We have not sorted these few cases out and show the result of the comparison in Fig. 4. For many sources, the flux density ratio is close to one, as expected, with an increasing scatter towards lower flux densities. There are a number of outliers. Figure 4 shows more sources with significantly higher flux densities in the Urumqi catalogue compared to the GB6 list, than for the opposite case. For sources with low flux densities, this effect is masked by the general scatter in the flux density ratio.

We have marked four "outlier" sources in Fig. 4 that show large differences in flux densities. We briefly discuss these cases to demonstrate the strengths and limitations of the different catalogues. All four sources are extended H II regions (Paladini et al. 2003) with small-scale structures measured with interferometers. Source 372 (l, b = 35.075, −1.494) has an integrated (peak) flux density of 5075 (3923) mJy in the present list and 8692 (1480) mJy in the GB6 source list. These flux density difference is clearly outside the errors of about 10%. The flux density ratio is 0.58 and thus exceptional low, see Fig. 4. The Effelsberg λ21 cm and λ11 cm catalogues list 6.27 ± 0.63 Jy and 6.47 ± 0.65 Jy integrated flux densities, respectively, consistent with the spectrum of an optically-thin H II-region. The present λ6 cm flux density seems to be slightly lower than expected, while the GB6 flux density is clearly too high. The much larger GB6 factor to convert peak flux into integrated flux density resulting from its smaller beam size seems to cause this inconsistency, which is connected to the uncertainties in the size determination. The other three sources 421 (l, b = 37.852, −0.331), 1144 (l, b = 79.284, 0.291), and 2429 (l, b = 150.378, −1.604) are "outliers" in the other direction, with a flux density ratio clearly exceeding 1 as seen from Fig. 4. The single-dish spectrum of source 421 is inverted up to 8.35 GHz (Langston et al. 2000), which indicates the presence of an optically-thick sub-component within the H II-region. The two other H II regions, sources 1144 and 2429, are optically thin. Numerous small components were detected by interferometers, which do not give the correct integrated flux density when summed up. The factor to convert peak into integrated flux density is near 2 for both sources and catalogues. The maps of these extended sources show a core-halo structure with a compact not always centred core. The obtained integrated flux density depends on the beam size to include the entire source. The almost identical Effelsberg λ21 cm and Urumqi λ6 cm beams imply that from these flux densities the most reliable spectra are obtained for extended sources.

5.2. The polarised sources

5.2.1. Distribution along the Galactic plane

The latitude distribution of polarised λ6 cm sources in the Galactic plane is nearly uniform. From the 125 sources, 61 have absolute latitudes below 2°.5 and 64 between 2°.5 and 5°. The longitude distribution, however, shows an increase in the number density with longitude: 51 sources are between 10° and 120° and 74 sources between 120° and 230°, which means that depolarisation and confusion is higher towards the inner Galaxy than for its outer region. For the survey section from 10° to 60°, Sun et al. (2011a) showed that the "polarisation horizon" is about 4 kpc at λ6 cm, otherwise the Galaxy is Faraday-thin. Among the polarised sources, there are both Galactic and extragalactic sources. Although the absolute number of polarised sources is small, the uniform distribution and missing concentration of polarised sources towards the Galactic plane indicates that the fraction of Galactic sources in the sample is quite small.

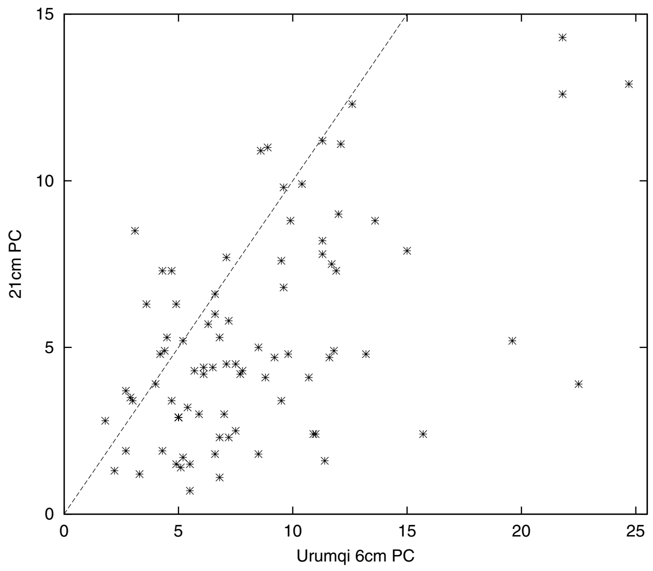

Fig. 5. Source percentage polarisation at λ6 cm versus λ21 cm.

We compared the number of polarised λ21 cm sources from the NVSS with an angular resolution of 45″ for the area of the λ6 cm survey observed with a 9.′5 beam. Since the majority of polarised sources is extragalactic with a mean non-thermal spectral index around $\alpha = -0.9$, a polarised λ21 cm flux density of 30 mJy corresponds to the 10 mJy polarised source limit at λ6 cm in case of no depolarisation. The number of polarised NVSS sources is 88, where 9 of them are double sources, which were not resolved with the large Urumqi beam. Thirty-two of the NVSS sources are between 10° and 120° and 56 sources between 120° and 230° longitude. The NVSS numbers are close to those from the Urumqi survey, which indicates that the angular resolution and the wavelength are not an important selection effect for sources with strong polarised emission. The NVSS lists about 20% more strong polarised sources (>30 mJy) for the entire longitude range, but for higher latitudes: 95 sources for +5° to +15° and 113 sources for −15° to −5°. The NVSS polarised source deficit in the Galactic plane refers entirely to the inner Galaxy, where the Galactic plane gets Faraday-thick (Sun et al. 2011a). This indicates that a line-of-sight of several kpc through the Galactic disk is needed to cause depolarisation of strong polarised signals on small scales. This changes for fainter polarised NVSS sources, where a latitude dependence exists. Selection effects of confusion with the fluctuating diffuse Galactic emission are more severe and have some influence on the detection of polarised sources.

5.2.2. Percentage polarisation

So far, no systematic survey for polarised sources at λ6 cm along the Galactic plane has been available. Thus, we compared the λ6 cm polarisation data with λ21 cm data from the catalogues listed in Sect. 4.2 and indicated in Table 2 as PC21. The polarised λ6 cm sources have 88 counterparts at λ21 cm. In most cases, the percentage polarisation, PC, increases towards the shorter wavelength as can be seen from Fig. 5, where λ6 cm PC is plotted versus λ21 cm PC. Faraday rotation depends on λ^2, and thus intrinsically highly polarised sources are seen to be more depolarised at λ21 cm than at λ6 cm. With few exceptions, the λ21 cm polarisation data are from high-resolution interferometric data, which resolve some single sources in the λ6 cm catalogue into two polarised components, but differential Faraday rotation within the sources is not resolved. The weak effect of Galactic differential Faraday rotation towards the inner Galaxy as taken from the source distribution discussed above indicates that the increase in the percentage polarisation at λ6 cm results mainly from decreasing internal source depolarisation.

5.2.3. Identification

Compared to the number of fitted total-intensity sources, the fraction of 125 Gaussian-fitted linearly polarised sources is just 3.3%. One may ask what is special to this small subgroup of sources that they are polarised, while the majority is not. We have used the VizieR service of the CDS for source identifications and found 32 extragalactic objects. Nine are Galactic and four sources might be SNR substructures or extragalactic sources projected against SNR shells. From the remaining 80 sources, 68 have spectra steeper than $\alpha = -0.6$, 3 have spectra flatter than $\alpha = -0.1$. This indicates that more than 80% of the polarised sources are extragalactic. Among the nine identified Galactic sources, six are SNRs, one is a planetary nebula, and two polarised objects were catalogued as H II regions. In principle, a H II region may depolarise and/or act as a Faraday screen when hosting a regular magnetic field component to rotate polarised background emission. This will cause a difference to the polarised emission in its surroundings. Such objects were discussed by Sun et al. (2007), including modelling, and also in other λ6 cm survey papers.

Source 627 (l, b = 50.192, 3.307) is identified with the flat-spectrum planetary nebula PK050+31 with an apparent diameter of 2′ at 688 pc distance (Stanghellini et al. 2008). The object might be similar to the planetary nebula Sh 2−216 discussed by Ransom et al. (2008) and might act as a Faraday screen in the same way as described for H II regions above. Because its distance is small, a large fraction of the polarised Galactic emission is located behind PK050+31 and gets rotated.

6. Concluding remarks

We present a list of 3832 compact sources extracted from the Sino-German λ6 cm polarisation survey of the Galactic plane, where 125 or about 3.3% of the sample are polarised. The λ6 cm survey complements earlier λ21 cm and λ11 cm surveys from the Effelsberg 100-m telescope with similar angular resolution and sensitivity. Most of the listed sources have counterparts at λ21 cm and λ11 cm, where the extension of the wavelength-range up to λ6 cm allows a more precise spectrum determination. It is of interest to determine the spectrum of H II regions at high frequencies, in particular, when they include compact optically-thick components. The identification of objects with spinning dust emission, which peaks between λ3 cm and λ1 cm, critically depends on reliable thermal emission spectra. The λ6 cm source catalogue lists about 20% more sources than the Effelsberg λ21 cm catalogue, which must be faint flat-spectrum sources. Their location in the Galactic plane suggests that most of them are faint H II regions, although confirmation is needed.

We compared the integrated flux densities from the Urumqi λ6 cm survey with those measured with the former Green Bank 300-ft telescope (GB6) with higher angular resolution. The integrated flux densities of extended sources seem to be more precise in the present catalogue.

We found a similar number and distribution of strong polarised NVSS sources at λ21 cm compared to polarised λ6 cm sources in the Galactic plane, despite their large angular resolution difference. The percentage polarisation increases from λ21 cm to λ6 cm. We conclude that the depolarisation properties of compact sources are mainly caused by internal effects, while small-scale Galactic Faraday effects do not contribute to the depolarisation except for the inner Galaxy with lines-of-sight of several kpc.

Acknowledgements. We thank Ernst Fürst for his support of the λ6 cm survey project and for critical reading of the manuscript. We acknowledge the help of Maja Kierdorf with source fitting and table editing. We are grateful to the staff of the Urumqi Observatory for qualified assistance with the survey observations. We thank Otmar Lochner for the construction, installation, and comissioning of the λ6 cm receiver. Maozheng Chen and Jun Ma helped with the receiver installation and maintainance during the survey project. The MPG and the NAOC supported the construction of the Urumqi λ6 cm receiving system by special funds. The Chinese survey team is supported by the National Natural Science foundation of China (10773016, 11303035) and the National Key Basic Research Science Foundation of China (2007CB815403). X.Y.G., L.X., and X.H.S. acknowledge financial support by the MPG, by Richard Wielebinski, and Michael Kramer during their various stays at the MPIfR Bonn. X.H.S. was supported by the Australian Research Council through grant FL100100114. This research has made use of the VizieR catalogue access tool, CDS, Strasbourg, France.

References

Broten, N. W., Macleod, J. M., & Vallé, J. P. 1988, Ap&SS, 141, 3038
Brown, J. C., Taylor, A. R., & Jackel, B. J. 2003, ApJS, 145, 213
Condon, J. J., Broderick, J. J., Seielstad, G. A., Douglas, K., & Gregory, P. C. 1994, AJ, 107, 1829
Condon, J. J., Cotton, W. D., Greisen, E. W., et al. 1998, AJ, 115, 1693
Fürst, E., Reich, W., Reich, P., & Reif, K. 1990a, A&AS, 85, 691
Fürst, E., Reich, W., Reich, P., & Reif, K. 1990b, A&AS, 85, 805
Gao, X. Y., & Han, J. L. 2013, A&A, 551, A16
Gao, X. Y., Reich, W., Han, J. L., et al. 2010, A&A, 515, A64
Gao, X. Y., Han, J. L., Reich, W., et al. 2011a, A&A, 529, A159
Gao, X. Y., Sun, X. H., Han, J. L., et al. 2011b, A&A, 532, A144
Gregory, P. C., Scott, W. K., Douglas, K., & Condon, J. J. 1996, ApJS, 103, 427
Han, J. L., Reich, W., Sun, X. H., et al. 2013, Int. J. Mod. Phys.: Conf. Ser., 23, 82
Haslam, C. G. T. 1974, A&AS, 15, 333
Kothes, R., & Kerton, C. R. 2002, A&A, 390, 337
Langston, G., Minter, A., D'Addario, L., et al. 2000, ApJ, 119, 2801
Paladini, R., Burigana, C., Davies, R. D., et al. 2003, A&A, 397, 213
Ransom, R. R., Uyanıker, B., Kothes, R., & Landecker, T. L. 2008, ApJ, 684, 1009
Reich, P., Reich, W., & Fürst, E. 1997, A&AS, 126, 413
Reich, W., Fürst, E., Steffen, P., Reif, K., & Haslam, C. G. T. 1984, A&AS, 58, 197
Reich, W., Fürst, E., Reich, P., & Reif, K. 1990a, A&AS, 85, 633
Reich, W., Reich, P., & Fürst, E. 1990b, A&AS, 83, 539
Reich, W., Fürst, E., Reich, P., et al. 2000, A&A, 363, 141
Rengelink, W., Tang, Y., de Bruyn, A. G., et al. 1997, A&AS, 124, 259
Sofue, Y., & Reich, W. 1979, A&AS, 38, 251
Stanghellini, L., Shaw, R. A., & Villaver, E. 2008, ApJ, 689, 194
Sun, X. H., Han, J. L., Reich, W., et al. 2007, A&A, 463, 993
Sun, X. H., Reich, W., Han, J. L., et al. 2011a, A&A, 527, A74
Sun, X. H., Reich, P., Reich, W., et al. 2011b, A&A, 536, A83
Tabara, H., & Inoue, M. 1980, A&AS, 39, 379
Van Eck, C. L., Brown, J. C., Stil, J. M., et al. 2011, ApJ, 728, 97
Vollmer, B., Gassmann, B., Derrière, S., et al. 2010, A&A, 511, A53
Xiao, L., Fürst, E., Reich, W., & Han, J. L. 2008, A&A, 482, 783
Xiao, L., Han, J. L., Reich, W., et al. 2011, A&A, 529, A15
Zhang, X., Reich, W., Reich, P., & Wielebinski, R. 2003, A&A, 404, 57

Pages 9 to 10 are available in the electronic edition of the journal at http://www.aanda.org

Table 2. List of compact polarised λ6 cm sources.

No	L (D)	B (D)	S_i (mJy)	S_p (mJy)	PI_p (mJy)	$\mathrm{PA_{gal}}$ (D)	$\mathrm{PA_{J2000}}$ (D)	PC_p (%)	Remark
34	12.425	3.846	1281	1209	76	176	116	6.8	PC21
35	12.447	–1.123	1467	1120	88	8	126	7.3	
101	18.379	–3.480	172	125	27	128	65	21.4	
107	18.593	–2.297	189	189	29	142	79	15.3	
193	24.973	4.401	486	424	24	109	47	5.7	QSO
232	27.301	3.516	134	104	21	37	154	20.2	
244	28.190	–3.992	76	46	10	165	102	21.7	
285	30.128	1.337	2042	1866	128	110	47	6.8	RadGal PC21
324	32.648	4.423	224	224	26	135	72	11.6	
379	35.486	–4.689	64	63	15	97	34	23.8	
388	36.014	–2.842	436	426	22	129	66	5.2	QSO PC21
439	39.233	–0.322	10334	7100	213	15	132	3.0	SNR G39.2-0.3
476	41.599	–2.924	330	330	21	5	123	6.4	
537	45.405	4.149	811	743	41	2	119	5.5	3C 394 PC21
621	49.999	1.779	113	92	18	27	145	19.6	PC21
627	50.192	3.307	214	201	13	27	144	6.5	PN
688	53.522	3.159	434	326	23	144	82	7.1	PC21
717	54.736	–0.099	1220	703	152	112	51	21.7	SNR G54.7-0.1
722	54.942	2.304	444	385	19	47	165	4.9	PC21
733	55.556	2.263	2300	2040	37	137	75	1.8	AGN PC21
742	56.093	0.108	317	289	17	3	122	5.9	QSO PC21
775	57.829	–2.354	161	152	15	157	97	9.9	PC21
796	58.766	0.650	358	209	12	0	119	5.7	HII
848	61.433	4.759	223	223	16	107	45	7.2	PC21
899	63.684	–2.334	472	472	42	148	90	8.9	PC21
906	64.051	–4.321	235	196	13	0	123	6.6	QSO PC21
938	65.288	–4.948	224	182	24	9	132	13.2	PC21
949	65.913	–4.591	252	252	12	84	27	4.8	AGN?
980	67.748	1.831	354	244	56	164	105	23.0	AGN?
993	68.587	–0.557	270	230	14	45	168	6.1	PC21
995	68.754	0.268	298	187	42	131	73	22.5	PC21
996	68.778	2.786	5282	3383	537	24	145	15.9	SNR CTB80
1004	69.209	–3.763	3682	3529	116	175	119	3.3	3C 410 PC21
1053	72.253	–0.974	1242	960	131	150	94	13.6	PC21
1085	74.944	1.156	7217	4571	221	155	99	4.8	SNR G74.9+1.2
1099	75.495	–3.130	152	78	12	60	7	15.4	
1120	76.883	0.959	714	500	20	14	139	4.0	SNR G76.9+0.9
1124	77.225	–3.237	429	341	22	168	116	6.5	PC21
1126	77.307	1.248	1075	783	38	178	123	4.9	PC21
1227	85.711	2.038	378	325	14	128	77	4.3	HII
1299	90.300	–3.782	306	254	18	132	88	7.1	PC21
1304	90.518	1.298	644	496	42	30	163	8.5	3C 468 PC21
1364	93.317	0.402	1499	1241	54	52	8	4.4	QSO PC21
1454	97.656	–3.543	622	552	15	8	151	2.7	QSO PC21
1552	103.281	–3.299	784	579	17	68	37	2.9	QSO PC21
1637	107.449	3.694	176	132	13	48	17	9.8	QSO PC21
1677	109.559	3.750	191	157	12	138	111	7.6	
1712	112.126	–4.488	273	220	25	160	142	11.4	PC21
1771	115.736	–1.082	128	106	12	51	38	11.3	PC21
1804	117.484	0.416	249	174	13	57	46	7.5	PC21
1823	118.546	–1.265	2021	1771	48	23	15	2.7	QSO PC21
1856	120.555	1.201	774	774	36	25	20	4.7	PC21
1867	121.212	–2.325	653	614	19	87	84	3.1	PC21
1881	121.889	–4.225	122	104	10	160	158	9.6	PC21
1924	124.335	4.850	275	211	22	0	3	10.4	PC21
2052	130.719	3.089	31286	25491	1210	149	165	4.7	SNR 3C58 PC21
2078	132.073	0.202	348	305	29	164	1	9.5	PC21
2105	133.886	4.377	433	433	37	98	122	8.5	AGN? PC21
2116	134.509	–2.006	221	171	12	176	16	7.0	PC21
2137	136.143	4.230	409	285	12	0	27	4.2	QSO
2139	136.211	–0.899	984	915	52	47	71	5.7	3C 69 PC21
2160	137.544	3.966	399	368	43	46	76	11.7	PC21
2211	140.120	–2.840	166	144	17	127	155	11.8	PC21
2223	140.875	2.430	197	168	12	82	115	7.1	PC21
2245	142.039	0.324	123	83	10	113	146	12.0	PC21

Table 2. continued.

No	L (D)	B (D)	S_i (mJy)	S_p (mJy)	PI_p (mJy)	PA_{gal} (D)	PA_{J2000} (D)	PC_p (%)	Remark
2276	143.496	–4.378	289	273	18	12	43	6.6	PC21
2283	143.895	–1.053	2830	2695	137	45	79	5.1	PC21
2295	144.431	0.908	184	109	12	30	66	11.0	QSO PC21
2305	144.982	–4.702	121	121	12	28	61	9.9	
2311	145.087	3.019	428	412	41	80	119	10.0	
2317	145.213	–2.337	1002	871	59	122	157	6.8	PC21
2336	145.953	–1.681	271	271	15	5	41	5.5	PC21
2353	146.933	–0.513	365	264	12	167	25	4.5	QSO PC21
2366	147.814	–3.898	1365	1245	52	163	19	4.2	PC21
2432	150.575	4.561	598	563	17	82	129	3.0	PC21
2440	150.857	4.536	291	252	27	81	128	10.7	PC21
2447	151.319	2.607	701	688	15	38	83	2.2	QSO PC21
2509	154.208	1.152	271	251	18	28	74	7.2	PC21
2519	154.677	3.377	257	228	15	27	76	6.6	PC21
2603	158.448	–4.253	380	301	29	151	16	9.6	PC21
2639	160.401	0.138	2443	1929	75	35	85	3.9	3C 129
2711	164.691	4.628	55	55	12	133	9	21.8	PC21
2761	167.640	–1.900	2157	1892	226	30	83	11.9	3C 134 PC21
2764	167.693	0.544	73	46	11	64	118	23.9	
2833	172.972	2.440	274	216	34	40	98	15.7	PC21
2857	174.369	–4.453	296	255	29	32	86	11.4	RadGal
2860	174.531	–1.319	526	526	57	168	44	10.8	3C 141
2930	178.832	2.646	410	324	13	36	96	4.0	PC21
2942	179.473	2.624	130	80	16	14	74	20.0	SNR-Shell
2966	180.746	0.955	389	337	31	39	98	9.2	PC21
2976	181.440	–2.125	119	70	17	112	170	24.2	SNR-Shell
3000	182.353	–0.623	349	300	23	72	131	7.7	PC21
3011	182.766	–4.942	101	101	14	18	75	13.9	
3047	184.467	3.045	294	271	26	58	119	9.6	
3070	185.592	4.002	1748	1541	66	136	18	4.3	3C 154 QSO PC21
3133	189.089	–4.045	328	302	13	30	89	4.3	PC21
3145	189.942	1.976	115	87	11	111	173	12.6	PC21
3148	190.126	–1.654	460	366	10	24	84	2.7	
3185	192.352	0.372	161	71	13	123	4	18.3	Origem Loop
3208	193.652	4.395	447	418	21	164	47	5.0	AGN PC21
3223	194.527	2.685	195	125	12	172	54	9.5	Origem Loop PC21
3241	195.863	–3.738	112	112	13	158	39	11.6	PC21
3251	196.329	–2.316	99	73	18	56	117	24.7	PC21
3254	196.587	3.197	1039	914	49	111	174	5.4	QSO
3260	197.062	0.323	84	80	12	26	88	15.0	PC21
3262	197.146	–0.860	771	740	65	146	28	8.8	PC21
3341	200.874	0.457	162	124	10	77	139	8.1	
3342	200.892	3.197	127	115	13	158	41	11.3	PC21
3364	202.184	–4.314	247	159	18	10	72	11.3	PC21
3416	205.415	–4.435	291	291	15	106	168	5.2	PC21
3424	205.799	4.905	182	166	13	48	111	7.8	PC21
3477	209.632	2.761	81	71	11	145	28	15.5	
3482	210.106	–2.635	260	213	16	47	110	7.5	PC21
3522	212.528	3.129	61	55	12	153	36	21.8	PC21
3533	213.130	0.553	212	182	22	37	100	12.1	PC21
3567	215.041	2.246	850	787	28	60	123	3.6	QSO PC21
3616	217.787	–3.011	301	196	12	66	169	6.1	QSO PC21
3622	217.958	4.249	406	367	20	62	125	5.4	PC21
3629	218.400	2.492	532	460	23	96	159	5.0	QSO PC21
3676	221.001	–4.688	187	187	16	176	59	8.6	PC21
3766	226.062	–1.767	135	110	11	11	74	10.0	
3767	226.073	0.383	153	119	13	108	170	10.9	PC21
3785	227.080	1.006	750	668	42	47	109	6.3	PC21
3795	227.583	–2.921	368	332	18	147	30	5.4	QSO
3810	228.367	2.552	78	78	12	59	120	15.4	